

Textured Electrodes: Manipulating Built-In Crystallographic Heterogeneity of Metal Electrodes via Severe Plastic Deformation

Jingxu Zheng,* Yue Deng, Jiefu Yin, Tian Tang, Regina Garcia-Mendez, Qing Zhao, and Lynden A. Archer*

Control of crystallography of metal electrodeposit films has recently emerged as a key to achieving long operating lifetimes in next-generation batteries. It is reported that the large crystallographic heterogeneity, e.g., broad orientational distribution, that appears characteristic of commercial metal foils, results in rough morphology upon plating/stripping. On this basis, an accumulative roll bonding (ARB) methodology—a severe plastic deformation process—is developed. Zn metal is used as a first example to interrogate the concept. It is demonstrated that the ARB process is highly effective in achieving uniform crystallographic control on macroscopic materials. After the ARB process, the Zn grains exhibit a strong (002) texture (i.e., $[002]_{Z_n}/ND$). The texture transitions from a classical bipolar pattern to a nonclassical unipolar pattern under large nominal strain eliminate the orientational heterogeneity of the foil. The strongly (002)-textured Zn remarkably improves the plating/stripping performance by nearly two orders of magnitude under practical conditions. The performance improvements are readily scaled to achieve pouch-type full batteries that deliver exceptional reversibility. The ARB process can, in principle, be applied to any metal chemistry to achieve similar crystallographic uniformity, provided the appropriate temperature and accumulated strains are employed. This concept is evaluated using commercial Li and Na foils, which, unlike Zn (HCP), are BCC crystals. The simple process for creating strong textures in both hexagonal and cubic metals and illustrating the critical role such built-in crystallography plays underscores opportunities for developing highly reversible thin metal anodes (e.g., hexagonal Zn, Mg, and cubic Li, Na, Ca, Al).

J. Zheng, Y. Deng, T. Tang, L. A. Archer Department of Materials Science and Engineering Cornell University Ithaca, NY 14853, USA

E-mail: laa25@cornell.edu
J. Zheng
Department of Physics
Massachusetts Institute of Technology
Cambridge, MA 02129, USA
E-mail: jkzheng@mit.edu
J. Yin, R. Garcia-Mendez, Q. Zhao, L. A. Archer
Robert Frederick Smith School of Chemical and Biomolecular
Engineering
Cornell University

Ithaca, NY 14853, USA
The ORCID ident

The ORCID identification number(s) for the author(s) of this article can be found under https://doi.org/10.1002/adma.202106867.

DOI: 10.1002/adma.202106867

1. Introduction

Metal electrodes have been widely deployed since the early 20th century to store energy in battery systems.[2,3] In their early forms, the batteries operated as single-charge devices-called primary batteries, e.g., AA alkaline battery (Zn-MnO₂).^[3,4] The recent decade witnessed a revival of research interest in metal electrodes that can work reversibly in rechargeable batteries.^[5] In this scenario, the metal is repeatedly plated and stripped during battery charge and discharge, respectively. The key issue faced by metal anodes in this new context is the formation of a heterogeneous, porous electrodeposition morphology that causes fast capacity fading and battery failure by various processes.^[6] These failure modes can be addressed in various ways by regulating deposition rate, electrolyte electrochemistry, interphase transport characteristics, and electrode geometry (e.g., nonplanar/3D electrodes),[6,7] but are understood to originate from fundamental characteristics associated with metal crystallization and dissolution processes that determine the reversibility of

the stripping and plating processes required to achieve long battery lifetimes.^[8–11] This has reintroduced a many-decades old challenge, which was attempted to be addressed by numerous investigators but remained unsolved before the development of intercalation battery electrodes^[12] allowed it to be ignored in pursuit of practical battery cells. The challenge is how to impose effective and sustained regulation on crystalline metal deposits at planar interfaces during repeated cycles of electroplating/stripping in a closed battery cell.^[10]

The porous, ramified electrode morphologies formed after repeated cycles of plating/stripping of a metal anode is now believed to stem from multiple fundamental instabilities, either physical (e.g., mass transport limit, uneven electrical field distribution), chemical (e.g., heterogeneous solid-electrolyte interphase), or an interplay of the aforementioned.^[9,13] The resultant complexity poses obvious challenges to the development of secondary batteries based on metal electrodes that can achieve





www.advmat.de

performance and lifetime operations at scale that are truly competitive (on either a weight or volume basis) with already commercial rechargeable battery technology based on intercalation electrodes. Very recently, a small number of works revealed that the crystallography of metal deposits plays a critical, but previously underexplored role in plating/stripping processes.[14-16] These studies showed that the crystallographic features of a metal deposit formed at the interface can serve as a sensitive indicator of the electrodeposition quality, including the geometry of the crystallite building blocks and the orientational order parameter with respect to the electrode surface. [9] A universal rule, independently established in different metal systems, e.g., Zn[14,17] and Li,[8,18] is that stable plating/stripping can be achieved when the deposits exhibit a strong crystallographic texture (e.g., as produced by aligning the close-packed crystal plane with the substrate). Multiple approaches for obtaining such textured metal deposits have been proposed, including heteroepitaxy, convective flow, electrolyte additive, and so on; it is remarkable that all appear to be successful in controlling the metal electrodeposit morphology during the plating process.^[10]

Noticeable is that these prior studies focus on metal deposition on substrates that are of chemistries different from the metal—such as Li on Cu,[18] Zn on carbon,[14] Zn on stainless steel, [19] etc., whereas in a deployable battery setup, the working anode is in the form of a thin metal foil pre-stored in the battery. The amount of the pre-stored metal typically exceeds-by at least one order of magnitude in most state-ofthe-art studies—the amount that is plated/stripped in each battery cycle. However, to be truly competitive with state-of-the art rechargeable batteries, nearly the full amount of the prestored metal must be utilized in each-and-every cycle of discharge and charge. This in turn means that the path toward practical metal anode batteries requires processes for creating extremely thin metal anodes that preserve the full electrochemical activity of the metal during the battery lifetime. It also means that the role the inherent crystallography of these metal foils play in the evolving electrode morphology cannot be overlooked. As we will soon see, the crystallographic heterogeneity of most commercial metal foils, featuring broad size and orientation distribution of the grains, externalizes itself through morphological and electrochemical instabilities that lead to battery failure during cycling. There are two fundamental origins of these instabilities. First, the dissolution rate of the metal is dependent on the exposed crystallographic facet.^[20,21] In other words, the orientational heterogeneity of the grains will translate into morphological heterogeneity upon battery discharge.[21,22] Second, electrodeposition on the metal foil is determined by homoepitaxy, [23] wherein the built-in crystallographic heterogeneity templates the morphology adopted by the newly deposited metal upon battery recharge. Therefore, strong interventions are needed to control the built-in crystallographic heterogeneities of the metal electrodes.

Using single-crystalline metals as anodes in batteries provides a number of advantages. The growth of single-crystalline metals has also been long pursued due to its technological importance—for example—in manufacturing turbine blades^[24] or condensed matter physics research.^[25] Unfortunately, the cost (\$100–1000 cm⁻²) and time needed to produce such high-quality single crystals at macroscopic scales, eliminates any

advantages, even the most cost-effective of these metals bring to energy storage technology—effectively ruling out existing approaches for producing such materials. Scalable, cost-competitive approaches for controlling the crystallographic properties of metal electrodes is consequently of interest both for fundamental reasons and for practical rechargeable batteries with long cycle life.^[26]

Severe plastic deformation (SPD) is a class of metallurgical processes in which a solid material is subject to a stress large enough to initiate plastic flow. The stress can be produced by processes such as rolling, extrusion, and forging that impose anisotropic deformations that are typically a combination of plane-shear and elongation. Application of these processes in metallurgy is well-studied and actively used to manipulate the microstructure of crystalline materials at the scale of a grain. [27] The important aspect of SPD relevant to the question defined earlier is that crystals undergo substantial texture evolution in an SPD process (see Figure 1).[28] SPD-induced texturing also exhibits strong dependence on the specific deformation procedures and the intrinsic crystal symmetry. This dependence is largely determined by the relative orientation of the principal deformation axis to the allowed slip planes for the material in question. The most conventional are cases where slip occurs preferentially at close-packed planes along the close-packed directions, e.g., (002) plane along <110> directions in hexagonal-close-packed (HCP) metals. This slip mechanism in HCP metals results in a characteristic texture of Normal Direction (ND) || <002>, also referred to as (002) fiber texture. [29] Of particular note is that, while texture evolution under plastic flow is a well-known effect, how to drive the material into a singly textured regime remains an open question.

Prior studies have shown that texturing of an HCP metal after rolling could be heterogeneous, i.e., significant amounts of (002), (100), and (101) textures coexist in the sample.[15] This suggests that, task-specific metallurgical deformation processes need to be designed in order to realize the strong texturing of interest here. One possibility is to exert greater strains by repeatedly rolling and folding the metal, also known as accumulative roll bonding (ARB, see Figure 1)—an advanced metallurgical technology.[30] This ARB process will allow arbitrarily large and temperature-dependent strains to be applied cumulatively to the material. In addition to this crystallographic aspect, the rolling-based plastic deformation also provides an approach for precisely manipulating the thickness of a metal foil (down to 10 µm). This serves as a knob to fine control over the amount of metal stored in the anode, and thereby achieve N:P ratios of interest in commercially relevant cell configurations.^[9,10,31] Here, we propose to take advantage of these fundamental principles and prior knowledge to manipulate the built-in crystallographic properties of metal anodes and, subsequently, illustrate the effect of the formed, highly textured materials, on morphological control during battery cycling.

As a first proof-of-concept demonstration, we choose Zn metal—a low-cost anode material that underpins multiple technological advances toward commercially competitive energy storage systems—to evaluate the roles played by crystallographic heterogeneity in electro-plating/stripping. The main rationale for choosing Zn is that it has an HCP crystal structure (see Figure S1, Supporting Information), which is thought to

www.advmat.de

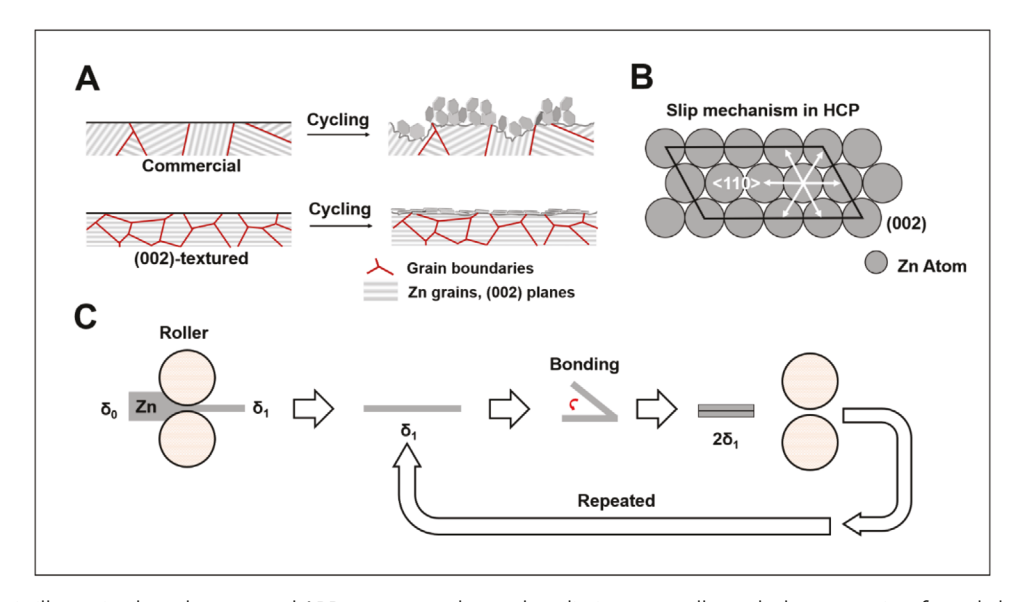


Figure 1. Schematic illustrating how the proposed ARB process can be used to eliminate crystallography heterogeneity of metal electrodes. A) Microstructures of the grains in as-obtained commercial Zn-metal foils (left), and the morphology after plating/stripping cycles in an electrochemical cell. B) Slip mechanism for HCP metals: (002) close-packed plane along <110> close-packed direction. C) Accumulative roll bonding (ARB) enables arbitrarily large nominal deformation reduction rate of metal foils. After each rolling pass, the as-rolled metal foil is folded (bonding) and then rolled again. A specified nominal strain can be achieved by repeating the roll-bonding cycles for a predetermined number of cycles.

correlate with a more anisotropic energy landscape than cubic crystals such as Li, Na, Al, etc. [9,32] A highly anisotropic energy landscape of Zn should also impose more explicit effects on the deposition morphology. Therefore, Zn serves as the appropriate candidate to evaluate the role crystallographic heterogeneity plays on the reversibility of plating and stripping processes inside a battery. Furthermore, Zn with a moderate electrochemical potential does not readily participate in parasitic chemical reactions as highly reactive alkali metals.^[33] This allows us to stay away from complications, such as the formation of a solidelectrolyte interphase, and to focus on the crystallographic aspects. Finally, from a metallurgical perspective, Zn has a relatively low melting temperature ($T_{\rm m}$) of 419.5 °C. As a result, the homologous temperature $(T_H)^{[34]}$ of Zn at room temperature is above 0.4 (i.e., $T_{\rm H} > 0.4$). This means that moderate ductility and softness is expected in Zn at room temperature, and high temperatures are therefore not required for Zn in order to avoid brittle cracking during rolling. This technical convenience greatly strengthens the technological impact the proposed concept could immediately generate. In Table 1, we summa-

Table 1. Temperature design of the plastic deformation process for candidate metals for battery anode applications.

| Metal | Melting point $T_{\rm m}$ [K] | 0.4 T _m [K] | $T_{\rm H}$ at RT |
|-------|-------------------------------|------------------------|-------------------|
| K | 337 | 135 | 0.88 |
| Na | 371 | 148 | 0.80 |
| Li | 454 | 182 | 0.66 |
| Zn | 693 | 177 | 0.43 |
| Mg | 923 | 369 | 0.32 |
| Al | 933 | 373 | 0.32 |
| Ca | 1115 | 446 | 0.27 |

rized the temperature criteria that can be used to design deformation protocols for other metal anodes of battery interest. As an empirical rule, it is generally accepted that plastic flow could be developed when $T_{\rm H}$ > \approx 0.4. [35]

2. Results and Discussion

Figure 2 reports the 2D X-ray diffraction characterization of the crystallographic features under different reduction rates (i.e., after different rolling passes). As is evident in Figure 2A, the commercial Zn-metal foil shows a broad size and orientation distribution. Three main diffraction rings are assigned to (002), (100), and (101), respectively. The simultaneous presence of the three rings (at the three 2θ angles) and the random γ angles of the spots on the rings together suggests a high degree of orientational disorder. The large variation in intensity of the diffraction spots is indicative of a broad size distribution—brighter, larger spots are generated by diffraction from coarser grains, and vice versa. As depicted in Figure 2A-D, the texturing of the metal foil undergoes remarkable transition as the effective strain increases (from the as-received foil #0, to foils after 8, 16, 24 times of ARB). Specifically, after 8 cycles of ARB, the Zn foil exhibits the classical bipolar distribution of (002) basal planes, featuring ≈15°-25° deviation from the normal direction of the foil. This is caused by Zn metal's large-scale twinning, in combination with the basal slip (002) <110>.[29]

As the nominal strain further increases, the Zn metal's texture transitions from the classical bipolar pattern slightly tilted away from ND toward the two transverse directions on the sides (e.g., #8),^[29] strikingly, to a unipolar pattern (e.g., #16, #24), as can be clearly seen in Figure 2A. This may be attributable to the nanosize of the grains as will be shown in **Figure 3**. Prior literature shows that the twinning in micrograins and nanograins

www.advmat.de

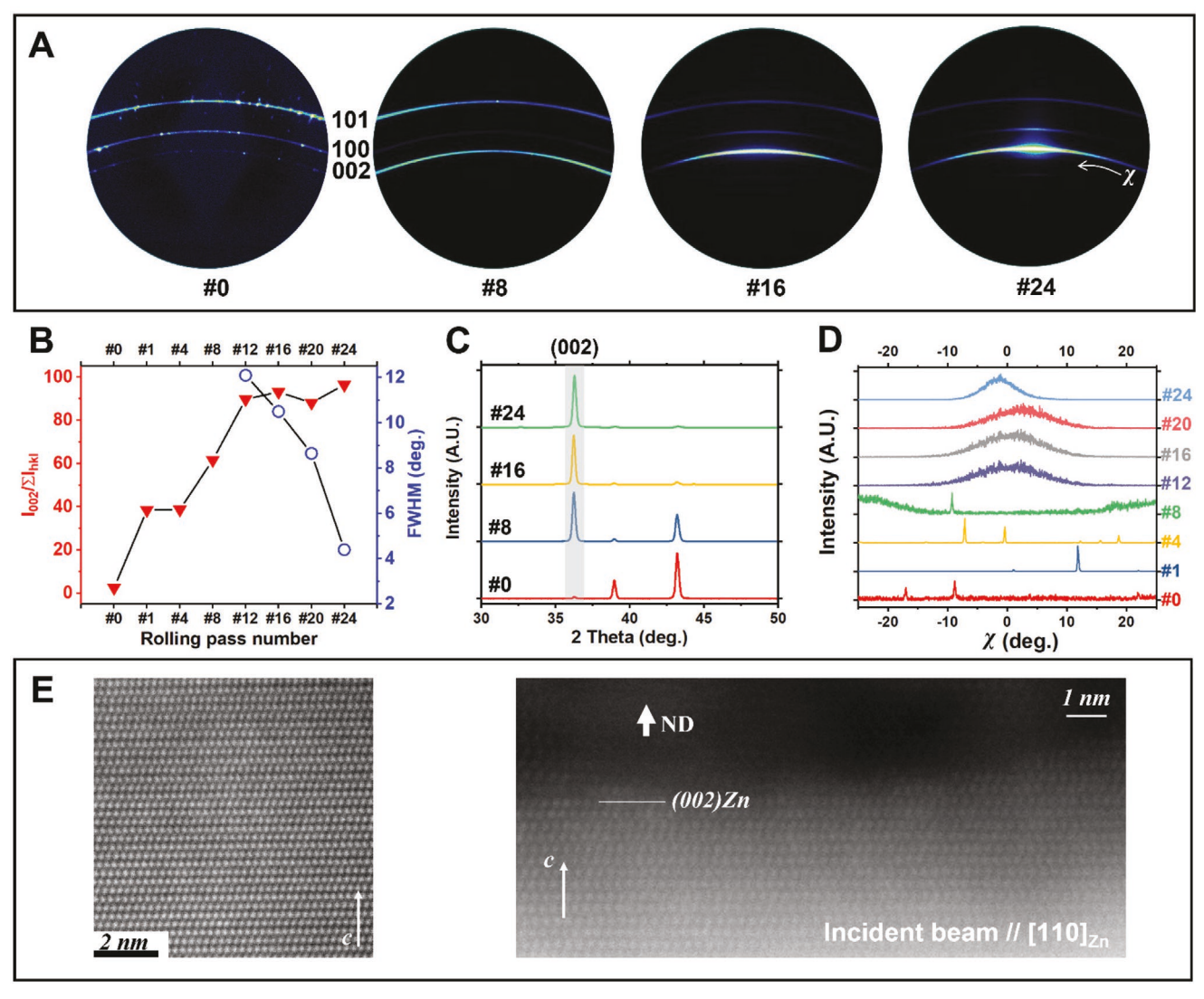


Figure 2. Crystallographic characterization of Zn-metal foils subject to ARB treatment. A) 2D X-ray diffraction patterns obtained for Zn foils before and after the number of accumulative roll bonding (ARB) cycles specified for each pattern (ω = 18.1°, 2 θ = 36.2°). B) Texture evolution during the ARB process. The red data points show the ratio between the (002) and total diffraction intensity. The blue data points show the full width at half maximum of (002) diffraction intensity along a range of χ angles. C) X-ray diffraction line scans. D) (002) diffraction intensity along χ angle. E) Cs-corrected HAADF-STEM images of ARB-treated Zn.

occurs via different mechanisms, and the critical stress value needed to initiate twinning in nanograins is significantly higher.^[36] Figure 2B–D provides detailed, quantitative analyses of such crystallographic transition processes. The ratio of (002) texture is observed to continuously increase and ultimately saturates at ≈90% after 12 times of ARB (see also Figure 2C; and Figure S2, Supporting Information). In the subsequent ARB process, the orientational distribution of (002) further narrows as quantified by the full width at half maximum (FWHM) of the (002) diffraction intensity peak along the χ angle. We further characterized the crystallographic structures of the Zn foils using advanced nanocharacterization techniques, including focused ion beam (FIB; see Figure S3, Supporting Information) and Cs-corrected high-angle annular dark-field scanning transmission electron microscopy (HAADF-STEM). Using an incident beam parallel to [110]_{Zn} zone axis, the HAADF images show that the Zn foil after ARB is strongly (002)_{Zn} textured (Figure 2E; and Figure S4, Supporting Information), whereas the as-received Zn foil is not (Figure S5, Supporting Information), consistent with the XRD analysis. The atomic-resolution imaging technique also provides additional information about the local, surface crystallography that XRD can not capture. A strong (002) texture does not guarantee a (002) surface termination if significant roughness is developed on the surface (see a schematic diagram in Figure S6, Supporting Information). The HAADF images in Figure 2E show that both the bulk and the surface of the sample is composed of $(002)_{\rm Zn}$ atomic planes parallel to the foil surface. Taken together, the X-ray diffraction and the HAADF-STEM imaging results unambiguously confirm that the built-in crystallographic heterogeneity of the Zn-metal electrode is strictly regulated via the ARB process as hypothesized earlier.

We employed optical microscopy techniques to characterize the metallographic features of the metal foils on larger length scales (Figure 3). Following standard metallographic characterization procedures,^[37] the metal foils are subjected to an

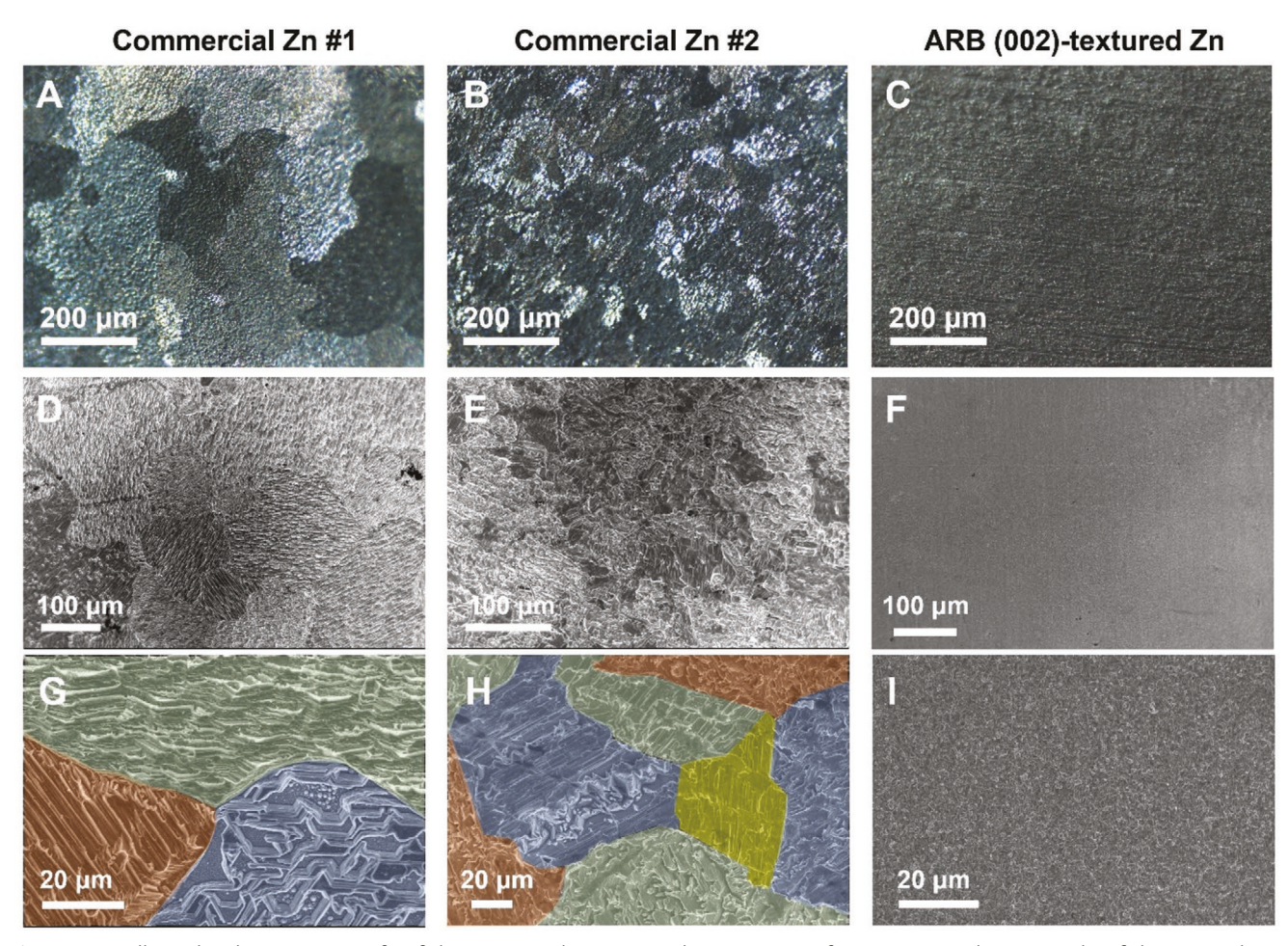


Figure 3. Metallographic characterization of Zn foils. A,B) Optical microscopy characterization of two conventional commercial Zn foils (A,B), and ARB (002)-textured Zn foil (C). D–I) Scanning electron microscopy characterization of the conventional Zn foils (D,E,G,H), and ARB (002)-textured Zn foil (F,I). The colored regions in (G,H) show different domains as identified by their distinctive surface topographies after etching. The foils are anodized (also known as "electropolished") before microscopy observation at 5 mA cm⁻² for 1 min.

electrostripping (polishing) process before observation to remove surface impurities and to unveil the landscape of the grains. In the anodization process, different facets show distinct dissolution rate, leading to a height variation across the grains with different orientations. Such height variation constitutes the contrast in optical microscopy images (Figure 3A-C). On two conventional commercial Zn foils, coarse grains with a large size and orientation distribution are observed (Figure 3A,B), in stark contrast to the uniform metallography of (002)-textured Zn foil (Figure 3C). This is consistent with the SEM observations showing the metallographic features at a smaller length scale. While the commercial foils exhibit large morphological heterogeneity after the electrostripping (Figure 3D,E,G,H), the (002)-textured Zn persistently show homogeneity down to the nanoscale. These metallographic characterization results corroborate the observations made based on X-ray diffraction, and also suggest that the (002)-textured Zn foil maintains the morphological homogeneity during electrostripping.

Next, the electroplating/stripping morphology evolution on metal foils of representative crystallographic features was evaluated. **Figure 4** shows the surface morphology of the Zn electrodes at multiple length scales after plating/stripping cycles in electrochemical cells using 2 M ZnSO₄(aq)—a mild-pH electrolyte

of interest in the development of commercially competitive Zn batteries. As can be clearly seen in the photos and optical microscopy images of the electrodes after cycling (Figure 4A-D), the Zn electrodeposits are grey, porous on commercial Zn foil, but shiny, compact on textured Zn foil. The origins of these two morphologies can be traced by examining the detailed growth mode of electrodeposited Zn on the foils. On the commercial Zn foil, the electrodeposit is comprised of randomly oriented Zn plates (Figure 4E), forming a porous network, which is widely reported in the literature, and detected on Zn deposits on inert stainlesssteel substrates. Without regulation, the intrinsic growth mode of Zn deposits is the assembly of randomly oriented Zn plates, which unfortunately leads to "dead"/"orphaned" Zn and subsequently, a battery short. On (002)-textured Zn foil, the Zn deposits remain in the plate-like morphology but are horizontally aligned with a compact deposition morphology. Chemical analyses show that the contents of oxygen and sulfur on ARB Zn after cycling are remarkably lower than commercial Zn (Figures S7 and S8, Supporting Information), suggesting a reduced parasitic reaction rate and a higher chemical stability of (002)-textured Zn. The comparison between the two morphologies suggests that homoepitaxy effectively dominates the deposition and promotes a uniform, planar surface morphology during cell cycling.

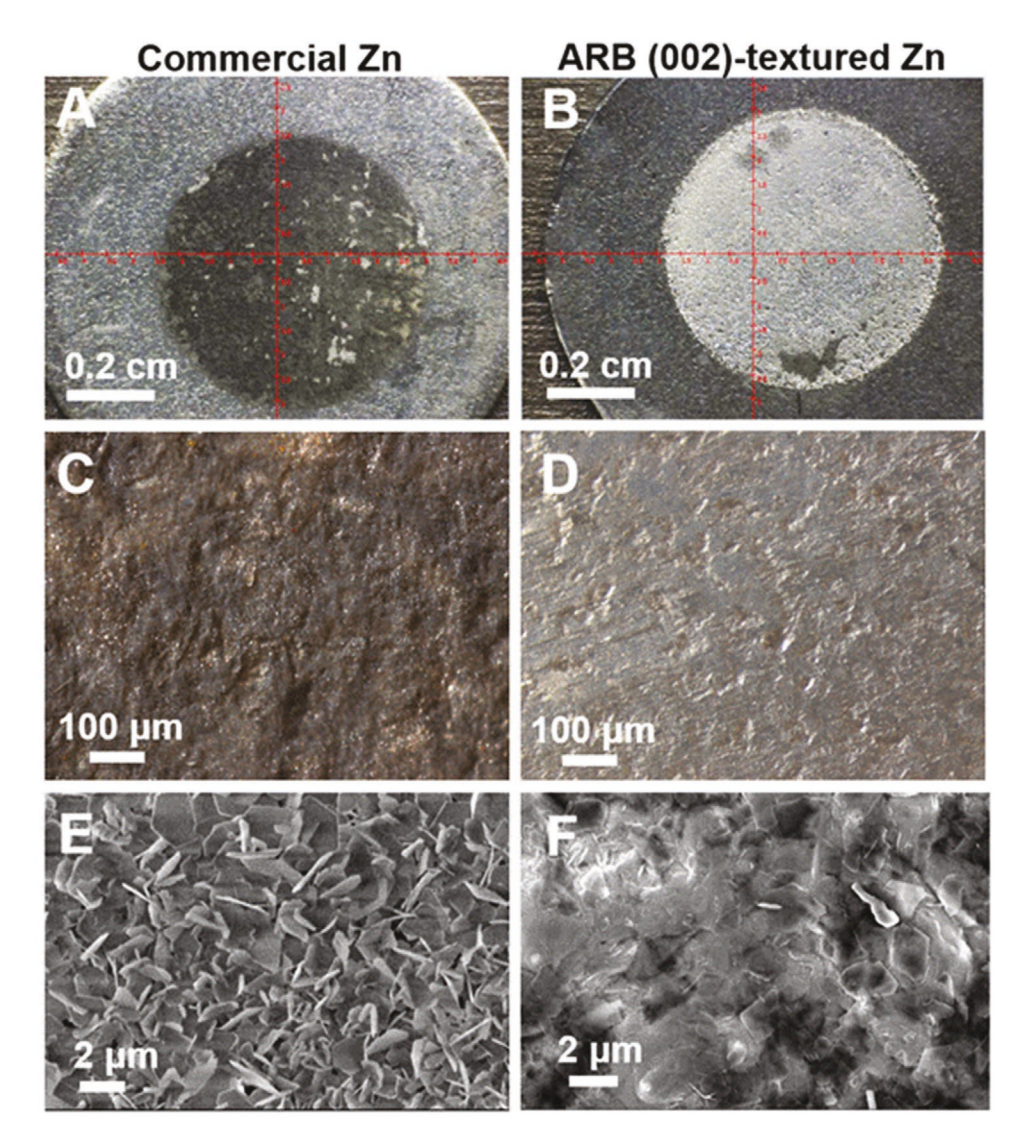


Figure 4. Surface morphology of Zn electrodes after plating/stripping cycles. A,B) Photos of cycled commercial Zn foil (A) and ARB-treated Zn foil (B). C,D) Optical microscopy images of cycled commercial Zn foil (C) and ARB Zn foil (D). E,F) Scanning electron microscopy images of cycled commercial Zn foil (E) and ARB Zn foil (F). Conditions: 8 mA cm⁻², 0.4 mAh cm⁻² for 10 plating/stripping cycles.

Following an established protocol reported in prior literature, we assembled Zn||Zn symmetric cells to assess the influence of built-in crystallographic features on the electrochemical cycling stability (Figure 5). A stringent cycling condition—areal capacity of 4 mAh cm⁻² at a current density of 40 mA cm⁻²—is chosen to ensure the measurement is of direct practicality. It is important to highlight that this pair of current density and areal capacity is at least one order of magnitude higher than state-of-the-art literature,[15,38] but is more relevant to commercially viable battery cycling conditions.[39] Results show that the cell using commercial Zn electrodes shorts in the very initial cycles, evidenced by the square-wave potential profile without any plating/stripping signatures (Figure 5A). The cells using (002)-textured Zn electrodes, in stark contrast, demonstrate stable plating/stripping behavior under this stringent condition over hundreds of cycles (Figure 5B-D). We attribute the gradual increase in cell overpotential and resistivity to hydrogen evolution (HER). It is caused by the intrinsic chemical instability of the water-based electrolyte (i.e., $\varphi(Zn^{2+}/Zn) = -0.76 \text{ V}$

vs standard hydrogen electrode) as evidenced by the increasing overpotential. HER manifests itself as a gradual buildup of gas and passivating side products on electrode surface, both of which contribute to the effective resistance of a battery and result in a greater observed overpotential. In this context, (002) Zn exhibits higher chemical stability and better corrosion-resistance due to its high atomic density, as recognized in multiple prior studies. Itaken together, this group of results show that no Zn deposit-induced instability (e.g., battery short) is observed. This argument is corroborated with results from coin-type and pouch-type full batteries shown as follows.

Motivated by the unprecedented electrochemical stability of the (002)-textured Zn electrodes, Zn full batteries were fabricated by pairing Zn electrodes with NaV₃O₈-based cathodes, prepared by a low-cost aqueous solution-based method. ^[42] In light of the scalability of both textured Zn anode and NaV₃O₈-based cathode, and the practical cycling conditions (i.e., high current density and areal capacity), we expect the results generated from these full cell battery studies to motivate fundamental,

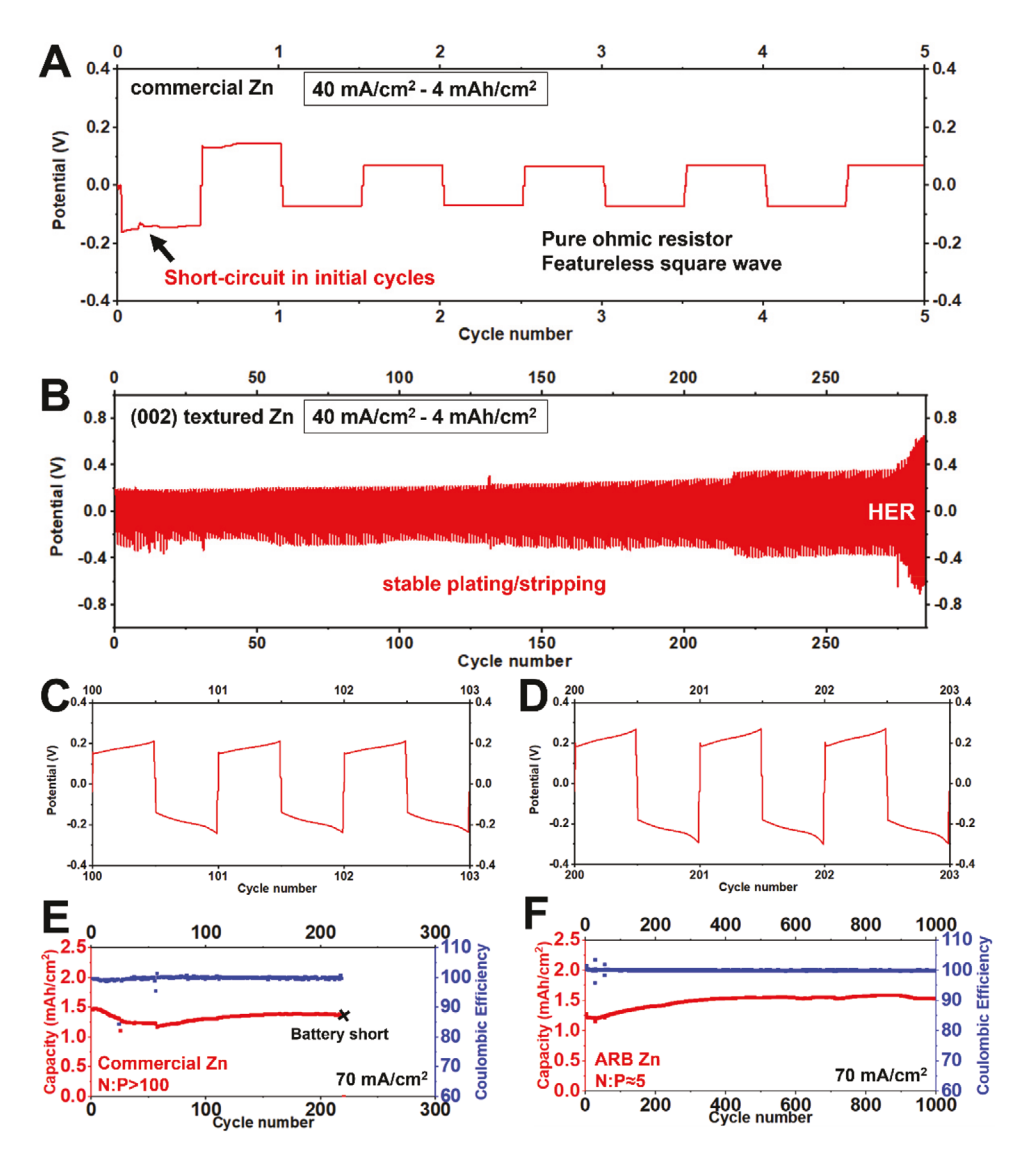


Figure 5. Electrochemical performance of Zn electrodes in symmetric battery cells. A,B) Plating/stripping cycling voltage profiles of commercial Zn foil (A) and ARB (002)-textured Zn foil (B). C,D) Detailed plating/stripping voltage profile of (002)-textured Zn foil after 100 cycles (C) and 200 cycles (D). E,F) Zn||NaV₃O₈ full batteries using commercial Zn electrode with N:P > 100 (E) and ARB (002)-textured electrodes with N:P \approx 5 (F).

technological, as well as commercial interest in the approaches reported. Figure 5E,F; and Figure S9 (Supporting Information) report results from aqueous Zn|| NaV3O8 battery cycling studies performed in CR2032 coin cells, as well as in pouch cells. Consistent with the symmetric cell experiment, full batteries using commercial Zn electrodes suffer from rapid fatal battery short events, whereas the ones using (002)-textured Zn electrodes exhibit impressive stability throughout prolonged cycling test. Particularly, full batteries using ARB Zn electrodes have a N:P ≈ 5, which is around two orders of magnitude smaller than the batteries using thick, commercial electrodes. It is found that the initial capacity of the battery using ARB Zn is slightly lower. This could be attributable to the known corrosion resistance of (002) facet of Zn;[21,41] that is, the crystal-facetdependent exchange current density j_0 of $(002)_{7n}$ is smaller. A slightly greater potential is needed to electrochemically dissolve (002)-textured Zn. It is believed that a smaller j_0 suppresses Zn's tendency for dendritic growth. [43] A smaller j_0 could improve

the chemical stability of the Zn electrode either in dynamic cycling or in storage. The stabilizing effect from the crystallographic homogeneity becomes even more pronounced in pouch cells (Figure S9, Supporting Information). We note that, the capacity fading observed in the prolonged cycling of full batteries using textured-Zn electrodes can be largely attributed to the water decomposition (i.e., HER) and gas buildup as reported in literature. [44] As a simple test, we observed that the capacity loss is fully recovered by refilling the electrolyte (Figure S11, Supporting Information). Therefore, the battery assessment reported here underscores the promise of textured metal anodes. Given the low N:P ratio reached by the thinning effect of the ARB process, it also opens up a robust technological pathway toward electrochemical energy storage systems that meet the levelized cost of energy storage (LCOS) requirement for integration into renewable energy harvesting systems, e.g., solar cells. [9,10,26]

Considering the common propensity of metallic crystals for undergoing texture evolution when subject to plastic

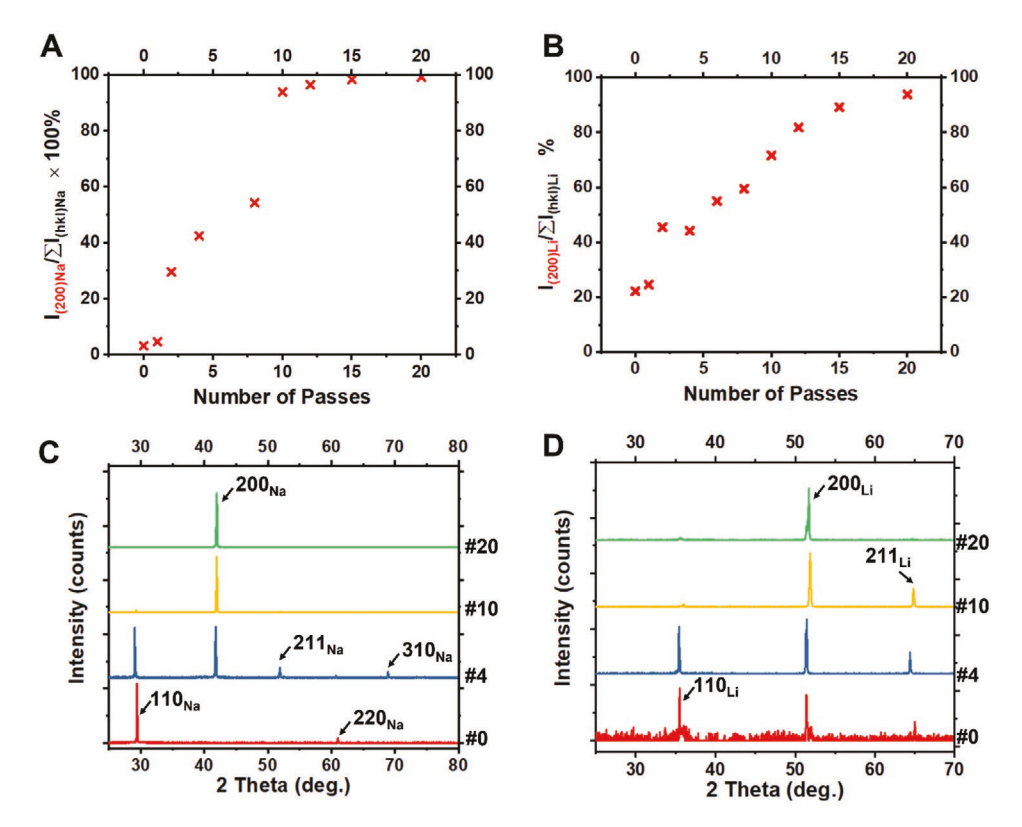


Figure 6. Crystallographic evolution in Na- and Li-metal electrodes subject to accumulative roll bonding. A,B) The X-ray diffraction intensity of (200) divided by the total diffraction intensity in the Na sample (A) and the Li sample (B). C,D) Representative 2θ line scans on the Na sample (C) and the Li sample (D).

deformation, the concept of ARB-induced strong texturing should be applicable to other metals that are under active consideration as candidates for high-energy-density anodes, e.g., Li and Na. The $T_{\rm m}$ of Na and Li are 97.8 and 180.5 °C, respectively. Similar to Zn, the relatively high $T_{\rm H}$ ensures their ductility and softness at room-temperature during the deformation process, which eliminates complications caused by brittleness and cracking. The major difference between Zn and Na/Li is that—the former belongs to a hexagonal crystal system, whereas the latter two have a body-centered-cubic lattice symmetry (see crystal structures in Figure S1, Supporting Information). Despite the difference in crystal symmetry, we conjecture that similar slip mechanisms should hold, i.e., close packed planes along close-packed directions. Figure 6 reports the texture evolution of Na and Li in ARB processes. Consistent with our expectations, it is observed that as the number of passes increases, both Na and Li exhibit stronger ND||<100> texturing. Such texture evolution phenomena are consistent with previous observations made on body-centered-cubic metals.[45] After 20 passes, foils of either Li or Na become singly oriented, featuring a uniform (100) texture throughout macroscopic sections of the sample (Figure 6). These results directly prove the general effectiveness of ARB for obtaining uniformly textured metal thin films suitable for battery anodes for hexagonal (e.g., Zn), and also cubic (e.g., Li and Na) metallic crystalline materials. We next examine the influence of the achieved crystallographic homogeneity on electrochemical behaviors by visualizing the surface morphology of the electrochemically anodized metal electrode (Li and Na, see Figures S8 and S9, Supporting Information). The strongly textured metal electrodes show a remarkably smoother interface than what is

formed on as-received electrodes. The smooth electrochemical interface on strongly textured Li/Na electrodes stabilizes the plating/stripping cycling of the metals (Figure S14, Supporting Information). These results show that, consistent with arguments based on Zn, the built-in crystallographic homogeneity plays a critical but oftentimes underexplored role in metal anodes that have cubic lattices (e.g., Li and Na). We further point out that, due to their smaller crystal anisotropy, the deformation texture of cubic metals shows a nontrivial dependence on specific deformation. As such, theoretical analysis could single out the possible texture components (see Table 2), whereas the

Table 2. Common rolling textures of metals. See more detailed discussions in the context of metallurgy in reference. $^{[l]}$

| Lattice | Texture (//ND) | |
|-----------------------|----------------|--|
| FCC (e.g., Al, Ca) | [111] | |
| | [110] | |
| | [112] | |
| | [001] | |
| BCC (e.g., Li, Na, K) | [001] | |
| | נווון | |
| | [110] | |
| | [112] | |
| HCP (e.g., Zn, Mg) | [001] | |
| | [100] | |
| | [110] | |



ADVANCED MATERIALS

www.advmat.de

actual deformation texture is probed by experimental methods. We note that, this relatively high degree of freedom associated with rolling texture of cubic metals creates substantial space for achieving task-specific textures that best stabilizes the plating/stripping process with carefully designing the deformation protocol.

3. Conclusion

We have reported severe plastic deformation (SPD) as an effective approach to eliminate in-built crystallographic heterogeneity in metal electrodes of interest for next-generation rechargeable batteries. As a proof-of-concept demonstration, we show that repeated rolling can significantly increase the (002) basal texture of HCP Zn metal, from <10% in conventional foils to >90%. We further show that as the nominal strain exceeds a critical value, the (002) texture of the Zn grains transition from the classical bipolar pattern to a unipolar pattern—a previously unexplored regime. The electrodeposition of Zn on the textured (002) electrode is dominated by compact, horizontal growth of the Zn plates, suggestive of a homoepitaxy process. This is in stark contrast to the porous, randomly oriented growth of Zn plates on commercial Zn foil. Cell cycling results show that the (002)-textured electrodes sustain hundreds of cycles under stringent testing conditions (e.g., 4 mAh cm⁻² at 40 mA cm⁻²), whereas cells using commercial electrodes short in the initial cycles. The findings reported here generate new perspectives for developing next-generation metal anodes for rechargeable batteries. The concept is extended to two other metals of contemporary interest, Li and Na, with very different crystallography and interfacial energetics in batteries. Remarkably, we find that SPD is as effective in creating uniformly textured films of both materials and that the texturing applies over macroscopic domains. The simplicity of our approach for manipulating the built-in crystallographic properties and the subsequent plating/ stripping reversibility achieved, should revive interest in other metals, e.g., Li, Na, K, Mg, Ca, Al, etc., that are of contemporary interest for next-generation secondary batteries.

Supporting Information

Supporting Information is available from the Wiley Online Library or from the author.

Acknowledgements

J.Z. expresses his gratitude to Prof. J. G. Checkelsky for invaluable discussion and support. This work was supported as part of the Center for Mesoscale Transport Properties, an Energy Frontier Research Center supported by the U.S. Department of Energy, Office of Science, Basic Energy Sciences, under Award No. DE-SC0012673. This work made use of the Cornell Center for Materials Research Shared Facilities which are supported through the NSF MRSEC program (DMR-1719875).

Conflict of Interest

The authors declare no conflict of interest.

Author Contributions

J.Z. and Y.D. contributed equally to this work. L.A.A. supervised the research. J.Z. and L.A.A. conceived and designed this work. J.Z. and Y.D. performed the deformation processing, structural characterization and electrochemical assessments of the electrode materials. J.Y. fabricated the cathode materials and the pouch-type full batteries. All the authors analyzed and discussed the data. J.Z., L.A.A., and Y.D. wrote the manuscript with inputs from all the authors.

Data Availability Statement

The data that support the findings of this study are available from the corresponding author (Prof. Lynden Archer) upon reasonable request.

Keywords

crystallography, plastic deformation, reversibility, secondary batteries, texturing

Received: August 30, 2021 Revised: October 7, 2021 Published online:

- S. Suwas, R. K. Ray, Crystallographic Texture of Materials, 1st Ed, Springer, Engineering Materials and Processes, London, UK 2014.
- [2] M. S. Whittingham, Science 1976, 192, 1126.
- [3] M. Friedman, C. E. McCauley, Trans. Electrochem. Soc. 1947, 92, 195.
- [4] a) E. Faegh, T. Omasta, M. Hull, S. Ferrin, S. Shrestha, J. Lechman, D. Bolintineanu, M. Zuraw, W. E. Mustain, J. Electrochem. Soc. 2018, 165, A2528; b) S. Bhadra, A. G. Hsieh, M. J. Wang, B. J. Hertzberg, D. A. Steingart, J. Electrochem. Soc. 2016, 163, A1050.
- [5] a) D. Lin, Y. Liu, Y. Cui, Nat. Nanotechnol. 2017, 12, 194; b) G. G. Yadav, J. W. Gallaway, D. E. Turney, M. Nyce, J. Huang, X. Wei, S. Banerjee, Nat. Commun. 2017, 8, 14424; c) D. E. Turney, J. W. Gallaway, G. G. Yadav, R. Ramirez, M. Nyce, S. Banerjee, Y.-c. K. Chen-Wiegart, J. Wang, M. J. D'Ambrose, S. Kolhekar, Chem. Mater. 2017, 29, 4819.
- [6] J. Zheng, T. Tang, Q. Zhao, X. Liu, Y. Deng, L. A. Archer, ACS Energy Lett. 2019, 4, 1349.
- [7] a) Y. Deng, J. Zheng, A. Warren, J. Yin, S. Choudhury, P. Biswal,
 D. Zhang, L. A. Archer, Adv. Energy Mater. 2019, 9 1901651;
 b) X.-B. Cheng, R. Zhang, C.-Z. Zhao, Q. Zhang, Chem. Rev. 2017, 117, 10403.
- [8] F. Shi, A. Pei, A. Vailionis, J. Xie, B. Liu, J. Zhao, Y. Gong, Y. Cui, Proc. Natl. Acad. Sci. USA 2017, 114, 12138.
- [9] J. Zheng, L. A. Archer, Sci. Adv. 2021, 7, eabe0219.
- [10] J. Zheng, M. S. Kim, Z. Tu, S. Choudhury, T. Tang, L. A. Archer, Chem. Soc. Rev. 2020, 49, 2701.
- [11] H. Liu, X. B. Cheng, R. Xu, X. Q. Zhang, C. Yan, J. Q. Huang, Q. Zhang, Adv. Energy Mater. 2019, 9, 1902254.
- [12] A. K. Stephan, Joule 2019, 3, 2583.
- [13] a) X. Wei, D. Desai, G. G. Yadav, D. E. Turney, A. Couzis, S. Banerjee, *Electrochim. Acta* 2016, 212, 603; b) D. Desai, X. Wei, D. A. Steingart, S. Banerjee, *J. Power Sources* 2014, 256, 145.
- [14] a) J. Zheng, Q. Zhao, T. Tang, J. Yin, C. D. Quilty, G. D. Renderos, X. Liu, Y. Deng, L. Wang, D. C. Bock, C. Jaye, D. Zhang, E. S. Takeuchi, K. J. Takeuchi, A. C. Marschilok, L. A. Archer, Science 2019, 366, 645; b) J. Zheng, J. Yin, D. Zhang, G. Li, D. C. Bock, T. Tang, Q. Zhao, X. Liu, A. Warren, Y. Deng, Sci. Adv. 2020, 6, 645.





www.advmat.de

- [15] M. Zhou, S. Guo, J. Li, X. Luo, Z. Liu, T. Zhang, X. Cao, M. Long, B. Lu, A. Pan, Adv. Mater. 2021, 33, 2100187.
- [16] D. Yuan, J. Zhao, H. Ren, Y. Chen, R. Chua, E. T. J. Jie, Y. Cai, E. Edison, W. ManalastasJr., M. W. Wong, *Angew. Chem.* 2021, 133, 7289.
- [17] T. Foroozan, V. Yurkiv, S. Sharifi-Asl, R. Rojaee, F. Mashayek, R. Shahbazian-Yassar, ACS Appl. Mater. Interfaces 2019, 11, 44077.
- [18] R. M. Kasse, N. R. Geise, J. S. Ko, J. N. Weker, H.-G. Steinrück, M. F. Toney, J. Mater. Chem. A 2020, 8, 16960.
- [19] S. Jin, D. Zhang, A. Sharma, Q. Zhao, Y. Shao, P. Chen, J. Zheng, J. Yin, Y. Deng, P. Biswal, Small 2021, 17, 2101798.
- [20] H. Asgari, M. R. Toroghinejad, M. A. Golozar, J. Mater. Process. Technol. 2008, 198, 54.
- [21] R. Ramanauskas, P. Quintana, L. Maldonado, R. Pomés, M. A. Pech-Canul, Surf. Coat. Technol. 1997, 92, 16.
- [22] W. Huaqing, Z. Shangqi, C. Changguo, W. Qiuhong, Chin. J. Chem. Eng. 2006, 14, 551.
- [23] X. Xin, K. Ito, A. Dutta, Y. Kubo, Angew. Chem., Int. Ed. 2018, 57, 13206
- [24] B. H. Kear, E. R. Thompson, Science 1980, 208, 847.
- [25] T. Suzuki, L. Savary, J. P. Liu, J. W. Lynn, L. Balents, J. G. Checkelsky, Science 2019, 365, 377.
- [26] Z. Yang, J. Zhang, M. C. W. Kintner-Meyer, X. Lu, D. Choi, J. P. Lemmon, J. Liu, Chem. Rev. 2011, 111, 3577.
- [27] R. Valiev, Nat. Mater. 2004, 3, 511.
- [28] S. Suwas, S. Mondal, Mater. Trans. 2019, 60, MF201933.
- [29] Y. N. Wang, J. C. Huang, Mater. Chem. Phys. 2003, 81, 11.
- [30] L. Jiang, M. T. Pérez-Prado, P. A. Gruber, E. Arzt, O. A. Ruano, M. E. Kassner, *Acta Mater.* 2008, 56, 1228.
- [31] a) L. Cao, D. Li, T. Pollard, T. Deng, B. Zhang, C. Yang, L. Chen, J. Vatamanu, E. Hu, M. J. Hourwitz, Nat. Nanotechnol. 2021, 16, 902; b) H. J. Peng, J. Q. Huang, X. B. Cheng, Q. Zhang, Adv. Energy Mater. 2017, 7, 1700797.
- [32] K. S. Nagy, S. Kazemiabnavi, K. Thornton, D. J. Siegel, ACS Appl. Mater. Interfaces 2019, 11, 7954.

- [33] a) X. Shen, R. Zhang, X. Chen, X. B. Cheng, X. Li, Q. Zhang, Adv. Energy Mater. 2020, 10, 1903645; b) R. Xu, X.-B. Cheng, C. Yan, X.-Q. Zhang, Y. Xiao, C.-Z. Zhao, J.-Q. Huang, Q. Zhang, Matter 2019, 1, 317.
- [34] J. Gubicza, N. Q. Chinh, T. Csanadi, T. G. Langdon, T. Ungár, Mater. Sci. Eng., A 2007, 462, 86.
- [35] J. E. Hockett, O. D. Sherby, J. Mech. Phys. Solids 1975, 23, 87.
- [36] a) M. A. Meyers, O. Vöhringer, V. A. Lubarda, Acta Mater. 2001, 49, 4025; b) D. Lahaie, J. D. Embury, M. M. Chadwick, G. T. Gray, Scr. Metall. Mater. 1992, 27, 139; c) M. A. Meyers, U. R. Andrade, A. H. Chokshi, Metall. Mater. Trans. A 1995, 26, 2881.
- [37] a) K. Geels, D. B. Fowler, W.-U. Kopp, M. Rückert, Metallographic and Materialographic Specimen Preparation, Light Microscopy, Image Analysis and Hardness Testing, ASTM International, West Conshohocken, PA, USA 2007, p. 46; b) R. Kovacheva, N. Gidikova, A. Lilova, Mater. Charact. 1992, 28, 205.
- [38] a) Y. An, Y. Tian, C. Liu, S. Xiong, J. Feng, Y. Qian, ACS Nano 2021; b) J. Hao, X. Li, S. Zhang, F. Yang, X. Zeng, S. Zhang, G. Bo, C. Wang, Z. Guo, Adv. Funct. Mater. 2020, 30, 2001263.
- [39] a) G. G. Yadav, J. Cho, D. Turney, B. Hawkins, X. Wei, J. Huang, S. Banerjee, M. Nyce, Adv. Energy Mater. 2019, 9, 1902270; b) G. G. Yadav, D. Turney, J. Huang, X. Wei, S. Banerjee, ACS Energy Lett. 2019, 4, 2144.
- [40] Y. Zhang, Y. Wu, W. You, M. Tian, P.-W. Huang, Y. Zhang, Z. Sun, Y. Ma, T. Hao, N. Liu, Nano Lett. 2020, 20, 4700.
- [41] N. Jantaping, C. A. Schuh, Y. Boonyongmaneerat, Surf. Coat. Technol. 2017, 329, 120.
- [42] F. Wan, L. Zhang, X. Dai, X. Wang, Z. Niu, J. Chen, Nat. Commun. 2018, 9, 1656.
- [43] D. A. Cogswell, Phys. Rev. E 2015, 92, 011301.
- [44] a) J. Shin, J. W. Choi, Adv. Energy Mater. 2010, 10, 2001386;
 b) M. J. D'Ambrose, D. E. Turney, G. G. Yadav, M. Nyce, S. Banerjee, ACS Appl. Energy Mater. 2021, 4, 3381.
- [45] M.-G. Lee, J. Wang, P. M. Anderson, Mater. Sci. Eng., A 2007, 463, 263.